

Robust Design and Optimization of Turbo-machinery Compressors

Preston Gomersall* and Devanshi Jain†
Undergraduate Research Hub, San Diego, 92122

Committed to advancing technology for a more sustainable and economically efficient future in air transportation, our research revolves around improving the capabilities of gas turbine engines. These engines are essential for operating commercial aircraft. This study specifically focuses on optimizing the compressor component within the turbine engine. The compressor section is crucial as it compresses air before it enters the combustion chamber. In this chamber, air undergoes fuel combustion, creating thrust needed for aircraft propulsion. Our research examines and fine-tunes key factors that impact compressor performance. These factors include blade twist angles, blade counts at each stage, and the clearance between shroud and hub tips. The goal is to enhance overall efficiency and performance. Our research methodology employs Ansys software, utilizing computational fluid dynamics (CFD) for detailed calculations. This enables us to create a comprehensive model, supported by various optimization tools integrated throughout the research process. Our study aims to contribute to the advancement of air transportation, ushering in a new era of greener and more cost-effective aircraft propulsion systems.

Nomenclature

BPR	By Pass Ratio	IGES	Initial Graphical Exchange Specification
CAD	Computer Aided Design	LPC	Low Pressure Compressor
EEE	Energy Efficient Engine	LPT	Low Pressure Turbine
HPC	High Pressure Compressor	N_c	Corrected Rotational Speed
HPT	High Pressure Turbine	NLH	Non-Linear Harmonic
ICLS	Integrated Core Low Spool	NPSS	Numerical Propulsion System Simulator

I. Introduction

Over the past decade, substantial attention and dedicated research has been directed towards enhancing the efficiency of gas turbine engines. Notably, the aviation sector is responsible for contributing approximately 2 percent of the total global greenhouse gas emissions. Presently, airlines are engaged in progressive endeavors involving the exploration of natural oils and novel fuel compositions, all aimed at mitigating the impact of greenhouse gas emissions. Concurrently, innovative initiatives are underway, involving the experimentation with advanced blade materials, exemplified by the utilization of cutting-edge carbon fiber composites. This particular carbon fiber technology has the capacity to withstand elevated temperatures and more formidable mechanical stresses.

In alignment with these industry-wide aspirations, our project undertakes a distinct focus on the meticulous selection of optimal geometries, blade counts, as well as the intricacies of hub and shroud curves, with the ultimate aim of refining fluid dynamics through a compressor. Our project utilizes the foundational geometry derived from NASA's Energy Efficient Engine (EEE) project, a publicly accessible blueprint originating from the pioneering work conducted during the 1980s at the NASA Glenn Research Center [1]. Computational fluid dynamics, which is computer simulations of how fluids flow, has drastically improved in the last decade. Our plan is to use these improvements to make the EEE model even more efficient.

*Undergraduate Student, Mechanical & Aerospace Engineering, pgomersall@ucsd.edu.

†Undergraduate Student, Mathematics & Computer Science, djain@ucsd.edu.

II. Background

In order to gain a comprehensive grasp of this paper, it is imperative to have foundational knowledge about turbofan and turbojet engines. A fundamental depiction of the core of a turbojet engine is illustrated in the figure below. The thermodynamic cycle that air undergoes within a turbojet engine involves a sequential progression through compression, combustion, turbine stages, and culminates in the converging-diverging nozzle.

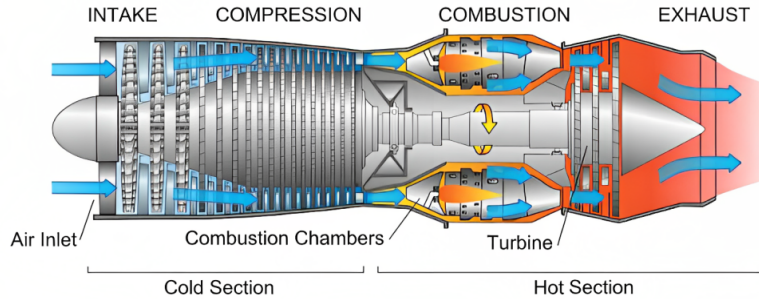


Fig. 1 This Figure represents the core of a jet engine

The process begins with the compression of air, a vital preparation for subsequent combustion. Optimal combustion transpires at elevated pressures and temperatures, facilitating superior fuel-air mixing and heightened reaction rates. The mixing of compressed air with fuel is followed by ignition through a spark, yielding thermal energy. This thermal energy is adeptly transformed into kinetic energy, inducing turbine rotation and propelling air rearward to produce thrust for the aircraft.

For our project we modeled a turbofan engine, which can be seen in the figure below. Turbofan engines have low and high pass compressor and turbine because the engine is split into two sections. The first section being the air that goes through the core of the engine and the second being the air that travels around the perimeter of the engine. The ratio between the amount of air that travels through the core, to the amount of air that travels around the exterior is called the By Pass Ratio (BPR). The BPR has a significant effect on the engine's efficiency. For a deeper insight into the intricacies of this phenomena, UCSD Professor Sanchez's annotations [2] on turbomachine engines, available in the references, offer valuable insight.

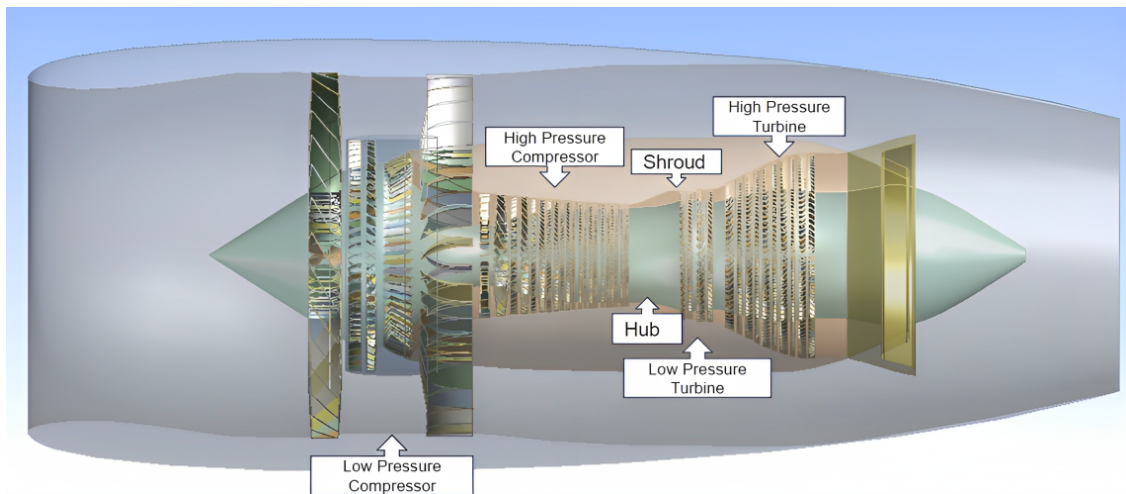


Fig. 2 Final updated geometry of the Energy Efficient Engine

III. Methodology

A. System Description

Our methodology involves the development of a turbofan geometry and the simulation of the engine's performance under cruise flight conditions at 35,000 feet and a flight speed of MACH 0.8. A pivotal aspect of our approach involves the utilization of Computational Fluid Dynamics (CFD) analysis, which enables us to delve deep into the intricate interactions of fluid flow within the compressor blades of turbojet engines.

Among various options in CFD simulation software, one stands out, as illustrated in Figure 3. Ansys's capabilities are underscored by its established accuracy, efficiency, and comprehensive functionalities. These attributes position Ansys as an optimal fit for the intricate task of turbojet engine optimization. The decision to employ Ansys expedites our product development timeline, enabling us to achieve efficient designs with a more streamlined approach.

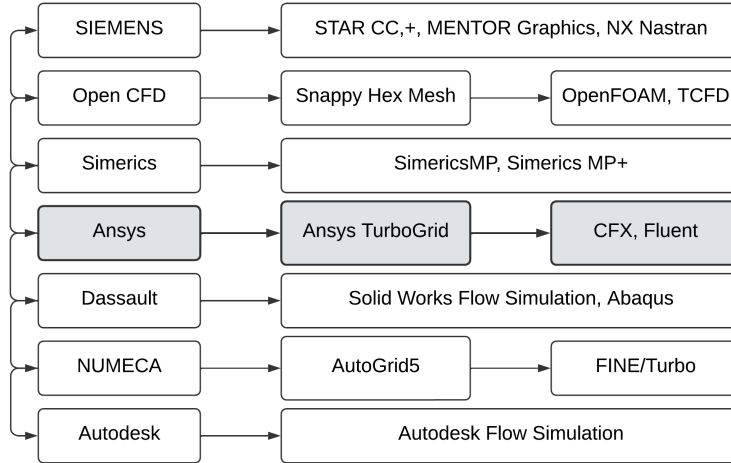


Fig. 3 Suite of CFD Simulation Software tools

B. Pre Processing

1. Process Overview

First we will give a brief summary of the entire process as depicted in Figure 4. The process begins by creating a meticulously designed geometry using Ansys DesignModeler. This geometry is then transformed into a surface mesh using the TurboGrid tool. Following this step, our focus shifts to CFX, where we set up the input and boundary conditions. The subsequent stages involve solving equations that define fluid flow such as the Navier-Stokes flow equations and analyzing the outcomes using CFD-Post.

Our approach delves deeper, encompassing a spectrum of input and output parameters within the domain of Response Surface Optimization (RSO). Through this iterative cycle, we refine modified geometries, construct meshes, and evaluate these adjusted design points. This iterative progression guides us in identifying optimal geometry configurations —ones that excel in enhancing the pressure ratio across each stage of the axial compressor.

This encapsulates a well-organized workflow that smoothly transitions through different stages, seamlessly integrating design, analysis, and optimization. The aim is to uncover the most effective configurations for enhancing the pressure ratio across the intricate arrangement of rotor-stator stages within the axial compressor.

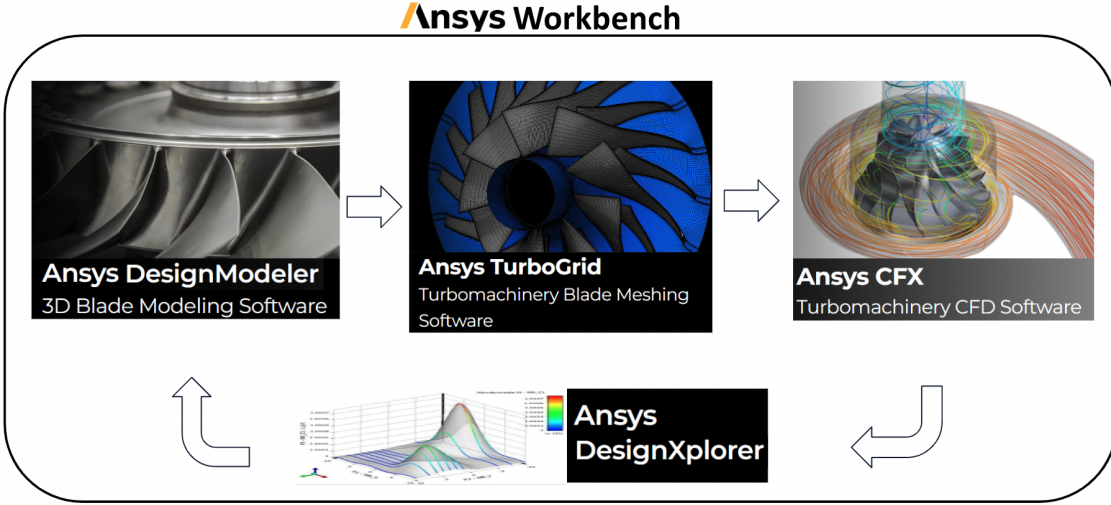


Fig. 4 Workflow set-up within Ansys Workbench using a suite of Ansys' turbomachinery tools

2. Geometry Modeling

Instead of creating the geometry of the axial compressor from scratch we utilized the NASA EEE [3] engine as our default geometry. Upon importing the geometry, we obtain the configuration depicted in Figure 5. This marks the initial setup within Ansys Design Modeler, encompassing 21 blades including the Inlet Guide Vane, followed by 10 subsequent stages of rotors and stators. To precisely define the geometry for each blade row in the engine, including the Low Pressure Compressor (LPC), High Pressure Compressor (HPC), High Pressure Turbine (HPT), and Low Pressure Turbine (LPT), we draw upon circumferential blade count data from Table in 2 which is provided in the same NASA paper [3].

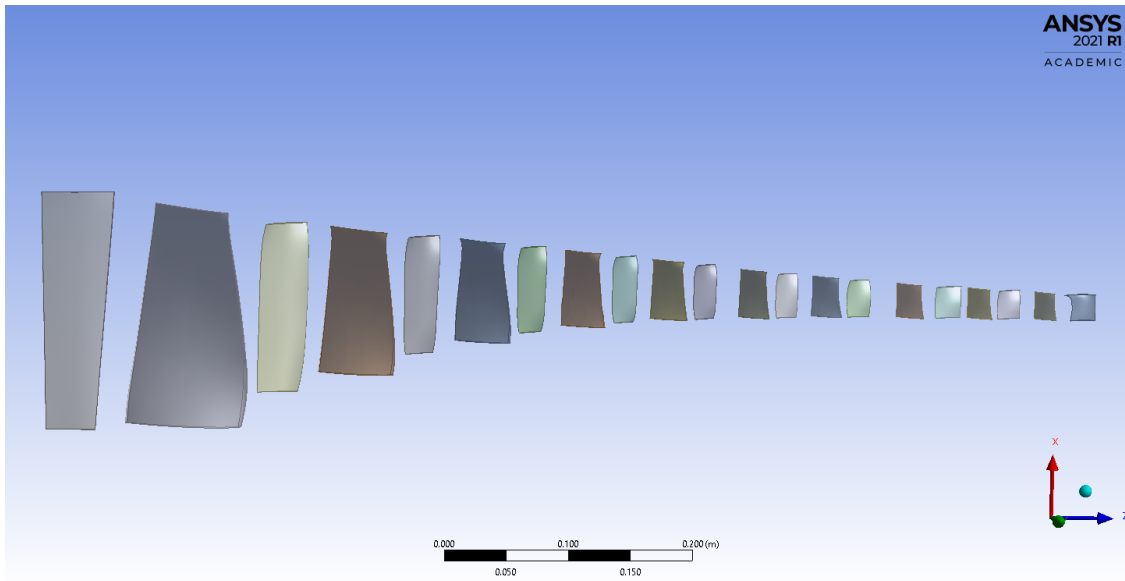
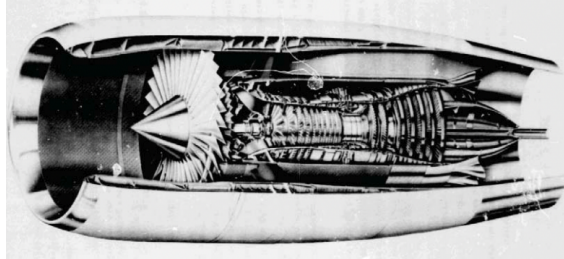


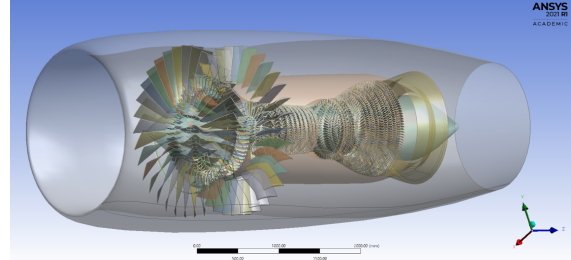
Fig. 5 Workflow set-up within Ansys Workbench using a suite of Ansys' turbomachinery tools

To prepare the geometry for simulation we created blades rows around the axial line of the engine, resulting in the intricate geometry portrayed in Figure 6b. This initial geometry exhibits striking parallels with the schematic of the General Electric's EEE shown in Figure 6a. The sequence portrays a distinct progression: commencing with the initial configuration of the Inlet Guide Vane, rotor, and stator blades, advancing through the integration of circumferential

blade count data, and culminating in the comprehensive initial geometry of the turbojet engine.



(a) Energy Efficient Engine developed by General Electric



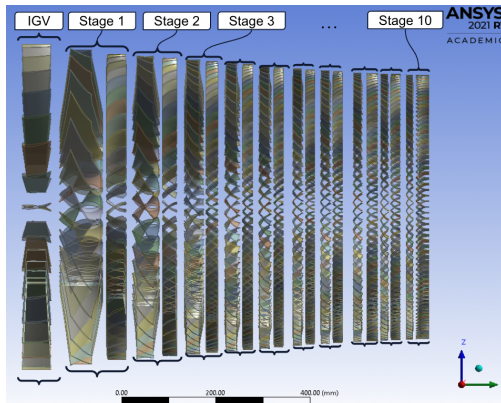
(b) Complete initial setup of turbojet geometry

Fig. 6 Physical and Computational Model of the Energy Efficient Engine

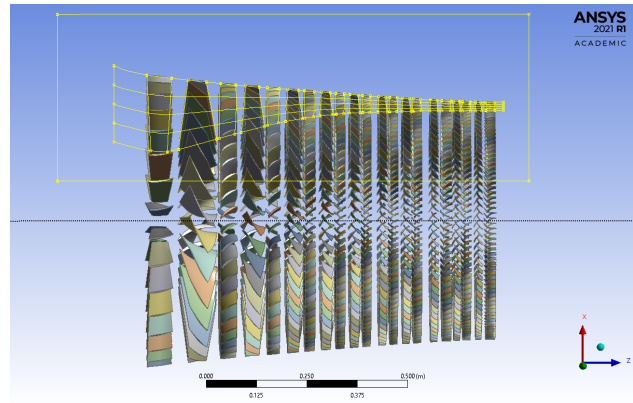
Following the establishment of the overall turbojet engine setup, our attention shifts to extracting the geometry of the axial compressor—a pivotal turbomachinery component central to our research. This axial compressor holds a critical role in increasing the pressure of incoming air, significantly influencing the engine's overall performance.

Within the axial compressor, three indispensable components assume distinct roles in facilitating the compression process for a 10-stage configuration, as elucidated by Figure 7a:

- **Inlet Guide Vane (IGV):** Positioned at the forefront of the compressor, the IGV functions as a vital air guide. Its primary task is to direct the incoming airflow, ensuring an optimized Angle of Attack (AOA) into the subsequent rotor stages. This strategic guidance lays the foundation for an efficient and seamless transition throughout the compression process.
- **Rotors:** These dynamic components, securely affixed to the hub or inner layer, play a decisive role in the compression journey. By propelling the air with heightened velocity, rotors induce a crucial increase in its kinetic energy. This enhanced velocity sets the stage for the subsequent phases of compression.
- **Stators:** In contrast, stators assume a stationary stance, adjoined to the shroud or outer casing. Their primary mission involves expertly guiding the airflow while concurrently reducing its velocity which in turn increases the pressure. This controlled deceleration is instrumental in preventing backflow and surge within the compression process, fostering both control and efficiency.



(a) Extracted 10-stage Compressor Geometry



(b) Flowpath Implementation on Compressor

The importance of designing a flowpath, carefully outlined by hub and shroud curves, becomes evident in Figure 7b. This process plays a crucial role in establishing a precisely defined inlet and outlet for every blade row. To enhance this process further, we incorporate three additional layers within the blades. This specific design enables us to introduce modifications and conduct comprehensive analyses at various blade areas.

To discuss more of the specifications of the geometry, we present the throat area of the first bladerow i.e. the IGV and last bladerow which is the tenth stator blade. the inlet area is 0.29

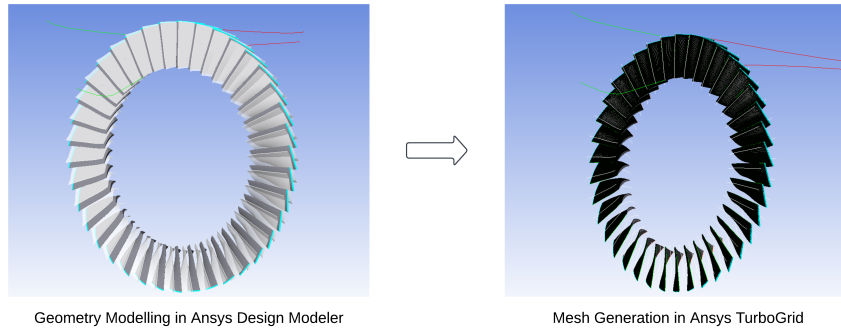


Fig. 8 Geometry to Meshing

3. Mesh Generation

We delve into generating high-quality blade passage meshes within axial compressors using Ansys TurboGrid [4]. These meshes play a pivotal role in accurately simulating real-world phenomena such as complex fluid dynamics and interactions between rotor and stator components. This section explores the process of generating high-quality meshes, a crucial step in ensuring accurate and reliable simulations.

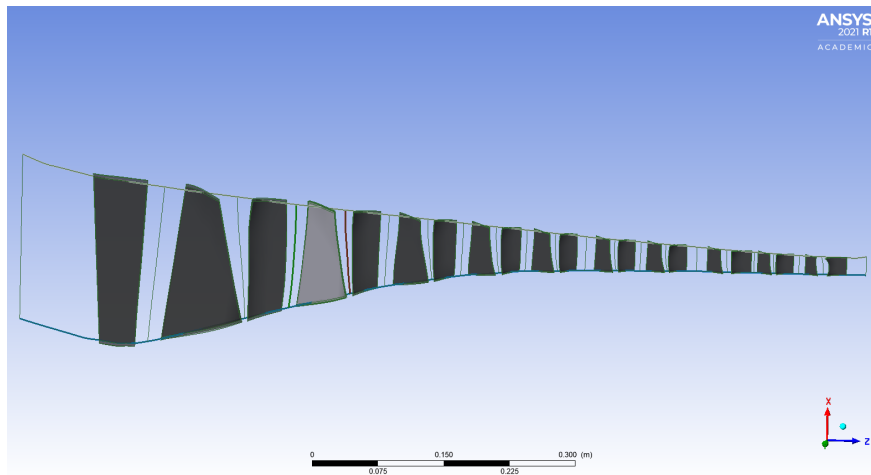


Fig. 9 Meshed Flowpath of the 10-Stage Axial Compressor

To begin, the flow path within the rotating machine is divided into specific volumes. We primarily use hexahedral elements, which have six sides and eight corners. In areas where the blade tip is situated, we introduce wedge elements. The positions of nodes at the corners of these elements form the mesh. This mesh covers the entire flow path and acts as input for the Ansys CFX solver that drives our simulations. The quality of the mesh directly affects the accuracy of our results.

We address gaps, particularly around the blade tips, utilizing predictive models to anticipate their impact on airflow. This enables us to optimize the mesh without excessive refinement. The mesh is dynamically created and adjusting itself based on the solution and geometry. These specialized models for gap areas provide accurate airflow predictions, ensuring our simulations stay within 5% of the actual values.

To ensure the mesh's quality, we analyze it using key parameters. These parameters include Minimum Face Angle, Maximum Face Angle, Element Volume Ratio, Edge Length Ratio, and Connectivity Number. This meticulous analysis ensures that the mesh meets strict quality standards, which is crucial for reliable simulations. Ansys TurboGrid efficiently computes the topology, and refined mesh for both hub and shroud layers. The topology is shown with dark pink lines and additionally serves as a background mesh to guide the creation of the refined mesh, denoted using fine lines. The mesh design seamlessly integrates a smooth transition at the blade tips, effectively bridging different mesh segments

Mesh Measure	Value	% Bad
Minimum Face Angle	56.92 [deg]	0
Maximum Face Angle	125.17 [deg]	0
Maximum Aspect Ratio	47.30	0

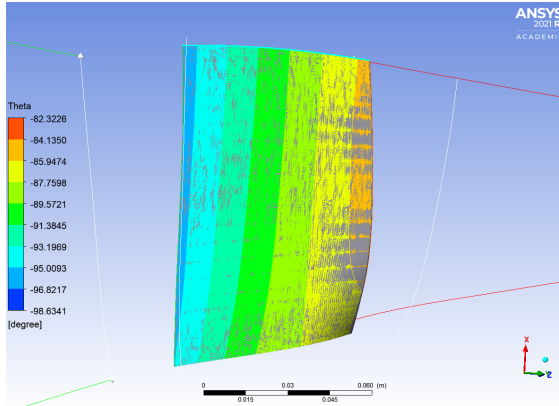
(a) Mesh Statistics for Shroud Tip

Mesh Measure	Value	% Bad
Minimum Face Angle	54.60 [deg]	0
Maximum Face Angle	116.03 [deg]	0
Maximum Aspect Ratio	36.80	0

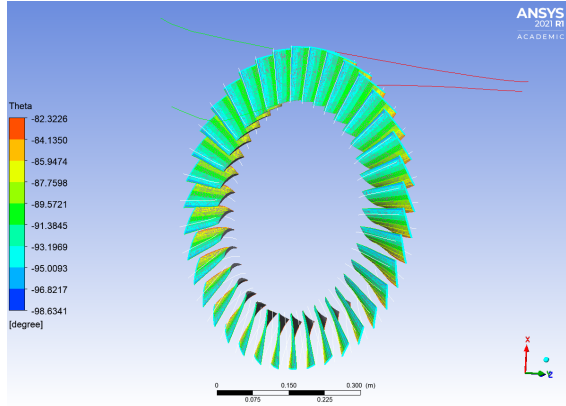
(b) Mesh Statistics for Hub

Table 1 Mesh Statistics of Rotor Bladerow's Shroud Tip and Hub

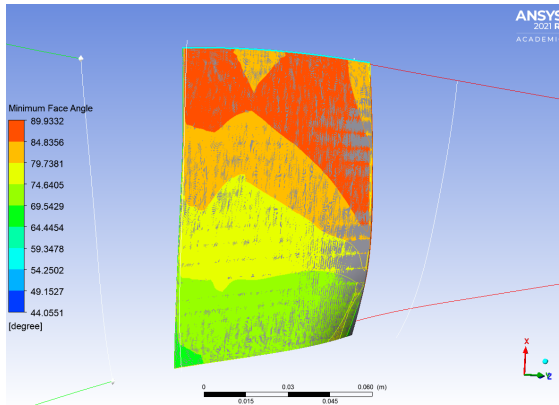
while employing a non-conformal mesh interface. This interface ensures compatibility and continuity within the mesh structure.



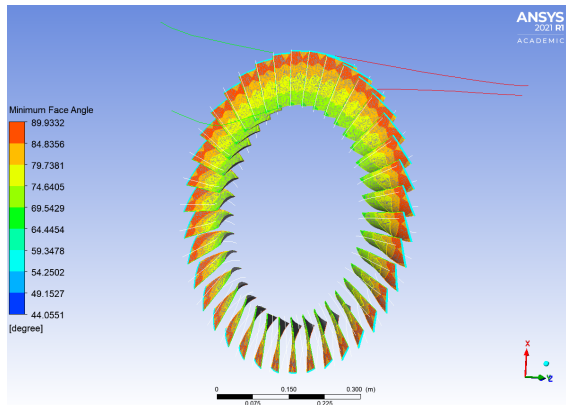
(a) Blade Curvature Theta Contour on a Rotor Blade



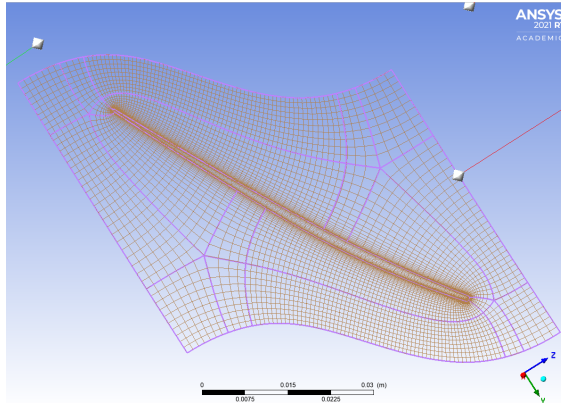
(b) Blade Curvature Theta Contours on a Rotor Bladerow



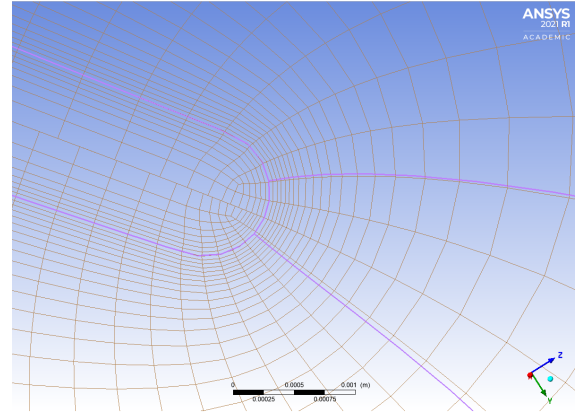
(a) Minimum Face Angle Contour on a Rotor Blade



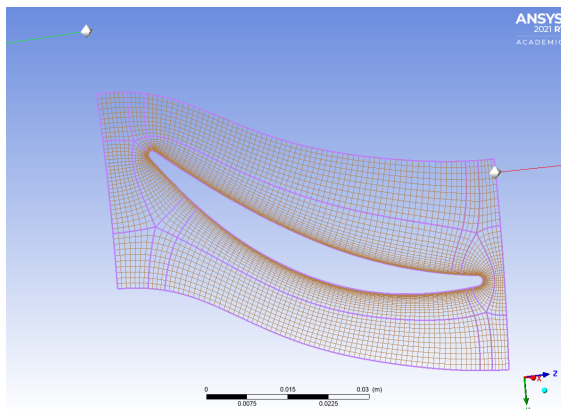
(b) Minimum Face Angle Contours on a Rotor Bladerow



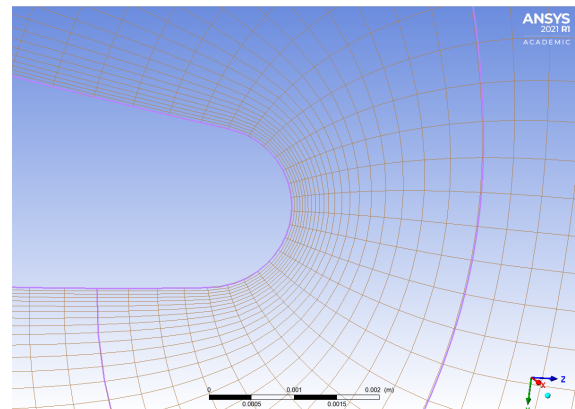
(a) Master Topology & Refined Mesh at Shroud Tip of a Rotor Blade



(b) Non-conformal mesh interface at Shroud Tip of Rotor Blade



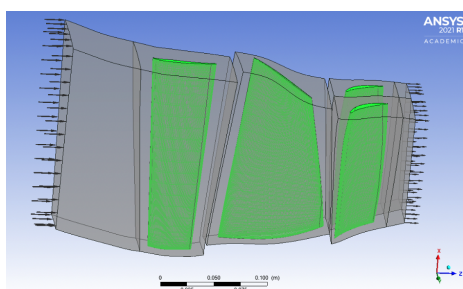
(a) Master Topology & Refined Mesh at Hub Region of a Rotor Blade



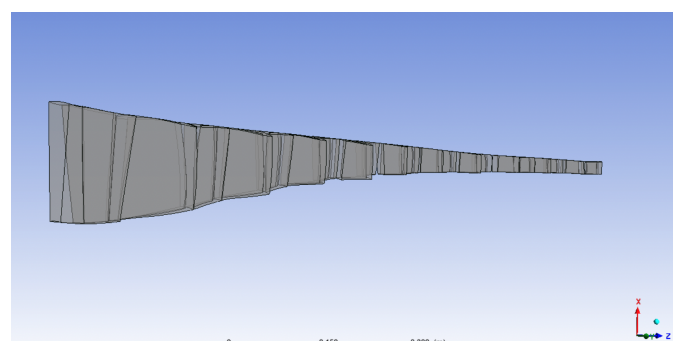
(b) Non-conformal mesh interface at Hub Region of Rotor Blade

4. CFX-Pre

In our effort to deeply understand turbomachinery dynamics, Ansys CFX has been an essential tool to thoroughly explore the aerodynamics, analyzing pressure losses, refining blade designs, and gaining insights into how the compressor behaves. With the help of refined mesh data, we fine-tuned simulation settings specifically for axial compressors within the ‘Turbo Mode’ in Ansys CFX-Pre. To configure the axial compressor’s arrangement we define 21 separate flow sections dedicated to IGV and the 10 pairs of rotors and stators to match each flow domain with their respective meshes. This alignment results in a comprehensive and realistic model of the system.



(a) Domain Interface Set-Up for a 1-stage compressor



(b) Domain Interface Set-Up for a 10-stage compressor

We meticulously set initial and boundary conditions to accurately capture the complex flow dynamics. Important

factors like pressure and mass flow rate were adjusted to mirror real conditions. The simulation operated at a steady 12000 rpm speed, maintaining a continuous mass flow rate of 64 kg/s. This virtual system closely mirrored reality, even reflecting an outlet pressure of around 200 psi. To capture turbulence effects precisely, we chose to use the K-omega model within the Reynolds-Averaged Navier-Stokes (RANS) framework. This decision allowed us to realistically replicate turbulent flow within the fluid dynamics of the system, a critical factor in the complex environment of turbomachinery.

Visual representation as presented in 14a and 14b show our setup's domain interfaces, offering a clear view of how the flow behaved across different sections. These visuals showed us the interactions within the initial three blade passages and also gave us a comprehensive understanding of the interfaces spanning the entire 10-stage axial compressor. To conclude, Ansys CFX was a key ally in our endeavor to comprehend turbomachinery intricacies. Ansys CFX-Pre set the stage for our exploration, while our simulations effectively depicted real-world behaviors.

C. Flow Solution

During the actual flow simulation, we employed a parallel run approach utilizing the computational power of 48 cores available through our lab's resources. Utilizing parallel processing significantly accelerated computation speed and overall efficiency, ensuring timely results. In axial compressor dynamics, achieving solution convergence is pivotal. This marks the point where iterative numerical solutions stabilize, with further steps causing minimal changes. The simulated flow and parameters settle into equilibrium, resembling steady fluid dynamics.

This convergence is a key reliability indicator. It reflects the alignment of numerical approximations, like Navier-Stokes equations, with set conditions, capturing complex flow interactions. Visual proof lies in solution converging graphs, affirming simulation fidelity and real turbomachinery behavior. It is noteworthy that our simulations achieved a convergence threshold of 10^{-4} , and the simulations were iterated over 300 cycles, indicating the robustness and accuracy of our computational approach.

D. Post Processing

During the post-processing phase, our emphasis shifted to data extraction and visualization in Ansys CFD-POST. The visual representation in Figure 15 provides an encompassing insight, showcasing velocity vectors, entropy, and Mach number contours at the 50% span position. These visualizations are pivotal for unraveling the intricate flow dynamics within the axial compressor. Examining the velocity vectors in Figure 15, a coherent pattern emerges. The velocity

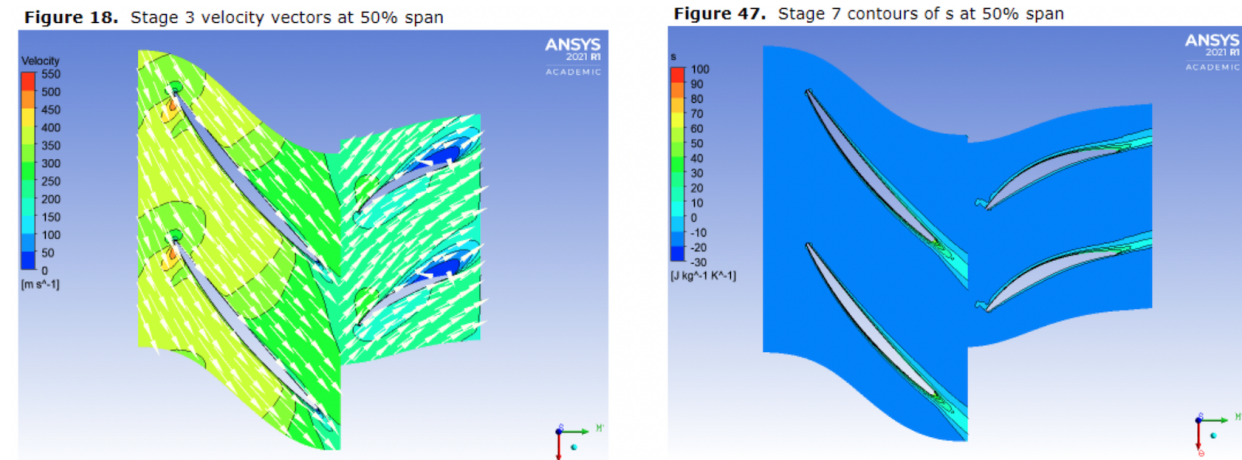


Fig. 15 Velocity Vectors and Entropy Contours at 50% Span

vectors provide a clear depiction of the flow direction and intensity within the rotor and stator pairs. The uniformity of the vectors illustrates the seamless continuity of the flow across these components, underscoring the functionality of the

axial compressor design.

The entropy contours, notably elevated at the tips, indicate regions of higher entropy generation. This observation implies potential energy losses associated with fluid mixing and diffusion, a common phenomenon in turbomachinery due to blade interactions.

IV. Results

Optimizing all ten stages of the axial compressor simultaneously posed a considerable challenge due to its computational complexity. To streamline the process, we adopted a sequential approach, meticulously addressing each stage individually. Our initial objective encompassed the enhancement of pressure ratios within the first stage of the axial compressor, encompassing the intricate interplay of the inlet guide vane (IGV), Rotor 1 (R1), and Stator 1 (S1). Through a comprehensive parameterization involving mass flow rate, rotor rotational speed, and outlet pressure, we successfully derived optimal conditions tailored to cruise flight scenarios for the axial compressor. The ensuing visual representation showcases the response surface obtained from an array of distinct design points that were executed.

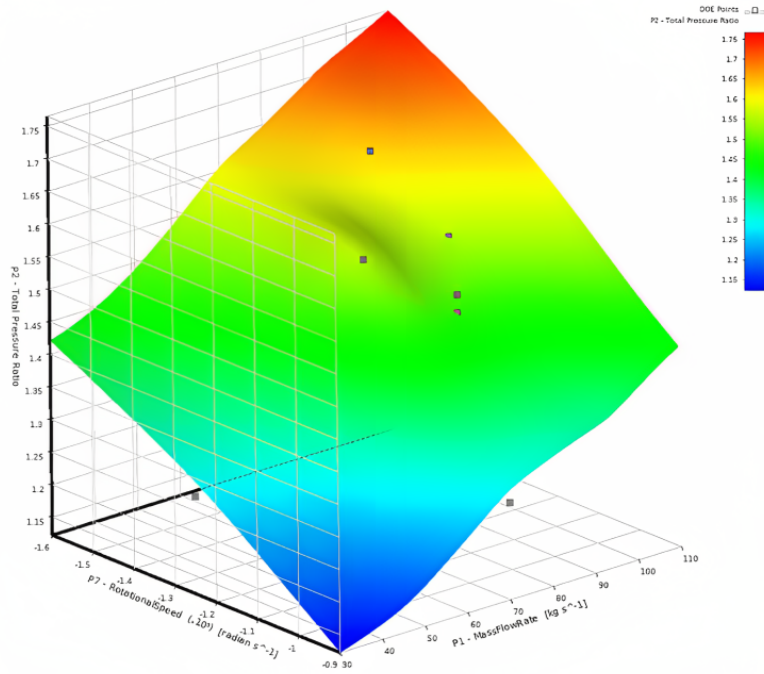


Fig. 16 This generated response surface for an axial compressor stage elegantly depicts mass flow rate (x-axis) and rotational speed (y-axis) as input parameters, with the paramount pressure ratio (z-axis) standing as our optimization focal point.

The idea behind conducting an array of design point experiments was to explore the engine's performance boundaries, identifying both its operational strengths and limitations. Leveraging these carefully gathered design points, we crafted a comprehensive compressor map, effectively delineating the extent of our compressor's capabilities. The accompanying figure below vividly illustrates critical parameters: the surge line and choke line, juxtaposed against varying compressor speeds. The surge line shows the point at which the pressure ratio attains levels that prompt reverse flow within the compressor. Conversely, the choke line denotes the threshold where an excessive mass flow rate overwhelms the compressor, resulting in a sharp efficiency decline and operational failure.

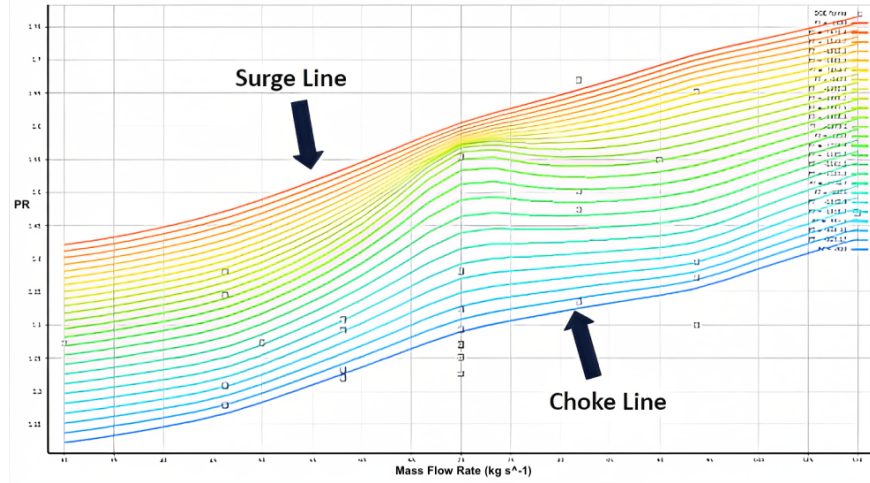


Fig. 17 This is an image of a compressor map in which the Surge Line and Choke line are represented by the top and bottom lines of the map.

Once we had a good grasp of how the airflow works best for the compressor during cruise flight, our team dug into how changing the number of blades and the space between the blades and the casing (tip clearance) could affect things. When you mess with the blade count in a compressor row, it changes the blade solidity for that stage, and that has a large effect on the pressure ratio. For our axial compressor the first group of stages deal with supersonic speeds at the blade tips, so that space between the blades and the casing becomes an important factor in how well the turbine works. Keeping that space in check turns out to be important in helping us sidestep issues like shockwaves, flow separation, and wave drag. The figure below shows the results of varying Blade count and shroud tip clearance for the first two rotors in the axial compressor.

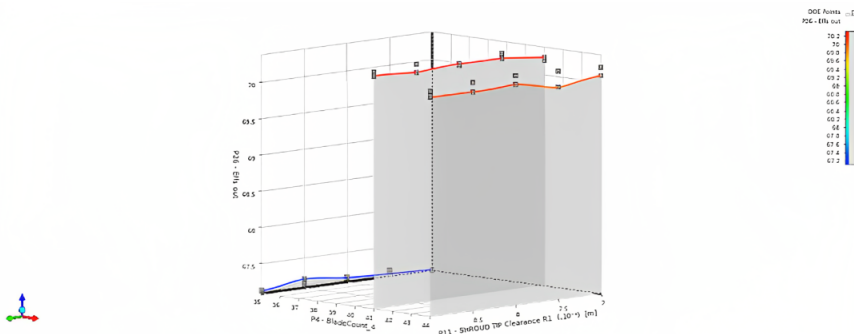


Fig. 18 Presented here is an illustration depicting the dynamic variation in blade count for the first-stage rotor. With the x-axis denoting tip clearance and the y-axis representing shroud tip clearance, the z-axis elegantly encapsulates our efficiency output, a pivotal gauge of performance.

The data in 18 makes it clear that the number of blades has a significant impact on the compressor's isentropic efficiency. To start with, the first rotor stage has 41 blades, and when you reduce the count to 35, the efficiency takes a noticeable reduction. As we look ahead, the use of advanced supercomputers will allow us to explore a wider range of design options for each rotor, helping us pinpoint the best blade count. This is a departure from our current method of estimating values between design points.

Subsequently, we worked to integrate the outcomes derived from our previous simulations, encompassing both axial compressor conditions and compressor geometry analyses. Leveraging Ansys' optimization tool, we harnessed input parameters to generate potential solutions aligning with our objectives. The ensuing figure beneath showcases the most promising candidate point gleaned from our meticulous simulation endeavors.

Parameter	Value
Mass Flow Rate (kg s^{-1})	41.701
Outlet Pressure (Pa)	200,170
Rotational Speed (radian s^{-1})	-1382
Total Pressure Ratio	4.2653
Stage 2 Total Pressure Ratio	1.7672
Stage 3 Total Pressure Ratio	1.7307
Stage 4 Total Pressure Ratio	1.2622
Stage 5 Total Pressure Ratio	1.2066
Total Temperature Ratio	1.723
Polytropic Efficiency Out	77.669
Isentropic Efficiency Out	73.061

V. Analysis and Conclusion

We successfully achieved the objective of enhancing the pressure ratio across the initial stages of the rotor. Nevertheless, there remains potential within this project for further enhancement. Notably, a crucial avenue for improving the project's precision would have involved conducting an unsteady simulation. The intricate interplay between the rotor and stator blades inherently manifests as an unsteady phenomenon, and the application of our current steady-state mixing plane model does not impeccably emulate the fluid dynamics.

Of particular significance is the incapability of the steady-state model to accurately represent shockwaves, especially those arising at supersonic Mach numbers. As illustrated in the diagram below, our observations indicate elevated Mach numbers at the tips of the rotor blades, which could potentially give rise to shockwave formations.

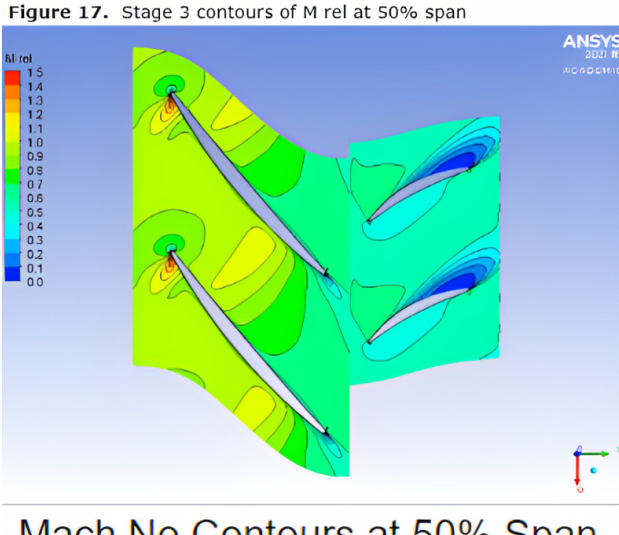
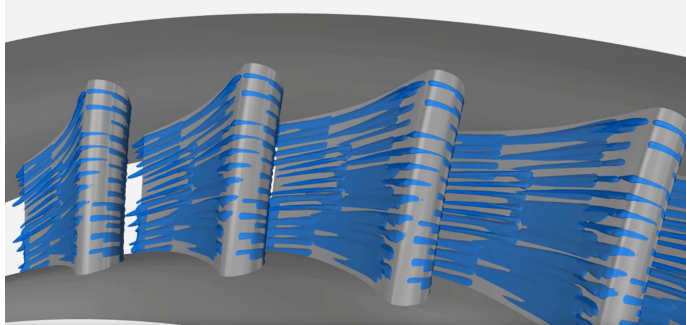


Fig. 19 Presented here is an illustration depicting the dynamic variation in blade count for the first-stage rotor. With the x-axis denoting tip clearance and the y-axis representing shroud tip clearance, the z-axis elegantly encapsulates our efficiency output, a pivotal gauge of performance.

An additional aspect that could have been incorporated into our modeling pertains to the inclusion of bleed valves. Upon examination of the figure provided above, it becomes evident that the gaps situated between the 5th and 7th stages serve as channels for the placement of bleed valves. The absence of these essential components had a large impact on the outcomes yielded by our comprehensive ten-stage simulations. This omission significantly influenced our decision

to concentrate solely on optimizing the initial four stages of the compressor.

Furthermore, our simulation could have also encompassed the intricate dynamics of the film cooling layer enveloping the rotor blades. This protective film cooling layer shown in the figure below, comprising a synergistic blend of oil and air, serves the crucial purpose of averting overheating and potential melting of the compressor blades. Given the elevated temperatures and pressures inherent to combustion processes, the durability of these blades can sometimes dictate the permissible operational limits. As elucidated in the introduction, ongoing experimentation with novel carbon fiber materials aims to fortify the blades against high temperatures, thereby ensuring resilience and longevity within the compressor's operational realm.



(a) Film cooling layer for a turbine blade following the combustion process. [5]



(b) San Diego Supercomputer on-campus at UC San Diego

With our newfound tools for modeling the axial compressor, we have the opportunity to extend our expertise to encompass additional engine components, culminating in a comprehensive module simulation. This expansion entails simulating not only the combustion process but also the intricate dynamics of the turbine blades. By doing so, we can propel our efforts towards enhancing engine efficiency, all the while gaining the ability to visually assess the impact of the optimized compressor on thrust generation.

Our research progress was primarily hindered by the challenge of connecting our project to the university's supercomputer. At UCSD, we have access to the EXPANSE supercomputer, which has the potential to run our design points on a much larger scale compared to the limited computational resources available in our on-campus CFD lab. With approximately 48 cores at our disposal in the CFD lab, we were constrained to running only about 30 design points. While this allowed for some optimization, being connected to the supercomputer could have enabled us to process thousands of design points in just a single day. In our future research we will incorporate the supercomputer with our research

Acknowledgments

We wish to express our sincere appreciation to the Undergraduate Research Hub's TRELIS program and its coordinator, Daniel Movahed, for sponsoring our research.

We are thankful to Professor Oliver T. Schmidt for supporting our research project. We extend special thanks to PhD student Edward Lowell for his invaluable guidance, unwavering support, and help with the Undergraduate Computational Modelling & Flow Physics Lab resources.

We also extend our gratitude to the San Diego Super Computer for generously allocating 200,000 ACCESS credits to support our project (ENG230006).

Appendix

Blade Row	Circumferential Blade Count
HPC Blade 1	32
HPC Blade 2	28
HPC Blade 3	50
HPC Blade 4	38
HPC Blade 5	50
HPC Blade 6	68
HPC Blade 7	82
HPC Blade 8	60
HPC Blade 9	92
HPC Blade 10	70
HPC Blade 11	110
HPC Blade 12	80
HPC Blade 13	120
HPC Blade 14	82
HPC Blade 15	112
HPC Blade 16	84
HPC Blade 17	104
HPC Blade 18	88
HPC Blade 19	118
HPC Blade 20	96
HPC Blade 21	140

Table 2 Circumferential Blade Count for Each Blade Row in the High Pressure Compressor

References

- [1] Holloway, P., Knight, G., Koch, C., and Shaffer, S., “Energy Efficient Engine High Pressure Compressor Detail Design Report,” NASA Technical Report CR-165558, NASA, May 1982. URL <https://ntrs.nasa.gov/api/citations/19850002690/downloads/19850002690.pdf>.
- [2] Sánchez, A. L., “An Introduction to Compressible Flow for Propulsion Applications,” <https://www.coursehero.com/file/189485720/Compressible/>, 2023. PDF notes.
- [3] Russell W. Claus, M. T., Tim Beach, Siddappaji, K., and Hendricks, E. S., “Geometry and Simulation Results for a Gas Turbine,” *AIAA Journal*, Vol. 24, No. 11, 2015, pp. 1872, 1873. <https://doi.org/10.2514/3.13046>.
- [4] Ansys, Inc., *Ansys TurboGrid User's Guide*, 2021. URL https://path-to-your-pdf-file/Ansys_TurboGrid_Users_Guide.pdf.
- [5] Ansys, Inc., “Design and Maintain Turbomachinery,” , Year of the article or publication. URL <https://www.ansys.com/blog/design-and-maintain-turbomachinery>.